Pergamon

Int. J. Heat Mass Transfer. Vol. 40, No. 4, pp. 961–971, 1997

0017-9310/97 $17.00 + 0.00

PII: S0017-9310(96)00155-X

Experimental study on the heat and mass transfer of a combined absorber–evaporator exchanger

YAU-MING CHEN and CHUNG-YUNG SUN

Department of Mechanical Engineering, National Taiwan University, Taipei, Taiwan 10764, Republic of China

(*Received* 21 *February* 1996)

Abstract—The present experimental study investigates the controlling mechanism involved in a new combined vertical film-type absorber–evaporator exchanger and deals with the experimental dependence of the overall heat and mass transfer rates on various operation conditions. The method of analogy between heat and mass transfer near the film surface is used to calculate the interfacial concentration and temperature, thus determining the heat and mass transfer coefficients. It is shown that the absorption process is controlled by a mass transfer mechanism on the liquid side and the mass transfer coefficients are higher than those obtained in isothermal absorption due to the convective effect arising from vapor absorption in the falling brine film. The correlations of mass transfer coefficient with respect to the inlet brine Reynolds number and physical properties have been derived. As to the heat transfer coefficient, it is found that the flow rate of water film and the absorber pressure have a minor effect on the overall heat transfer coefficient of the whole unit. In addition, a predictive model, based on the superposition of heat transfer near wall and near film surface, is proposed and has been successfully applied to evaluate the heat transfer coefficient of the absorber itself. Copyright © 1996 Elsevier Science Ltd.

1. INTRODUCTION

The interest in absorption of water vapor on brine solution originates from the idea of energy recovery. Actually, concentrated salt brines represent a large source of stored energy and are naturally available in various locations around the world. Isshiki [1] initiated a power cycle which utilized the concentration difference energy (CDE) unit, wherein the heat of dilution and the boiling point elevation of concentrated brines were used to drive the heat engine, schematically depicted in Fig. 1. However, this unit needs two heat exchangers for high and low temperature levels, respectively, thus lowering the nominal driving force available for power generation. In order to improve this disadvantage, Brauner *et al.* [2, 3] proposed a direct-contact CDE power cycle scheme, as depicted in Fig. 2, wherein the heat released during direct contact hygroscopic condensation on the brine solution sustained the continuous generation of upgraded vapor to drive the turbine. Continuous energy transport in this process is possible because the latent heat of vapor absorption on a hygroscopic salt solution is relatively higher than that of evaporation of pure water.

Cheng [4] proposed a similar process in waste water treatment and chemical purification. The vapor pressure enhancement, which is the main purpose of such a process, is accomplished across a vertical heat transfer wall provided with two falling liquid films. The film on one side is an absorbing solution while on the other side is pure water. The first vapor brought in contact with the relatively hot solution film is absorbed due to the reduced vapor pressure of the salt solution. The heat released is transmitted through the vertical wall to vaporize water on the other side and generates a second vapor whose pressure is higher than that of the first vapor.

The non-isothermal heat and mass transfer characteristics of the simultaneously direct-contact absorption–evaporation unit are of major importance in evaluating the overall performance of the systems mentioned above. The main problem in calculating the overall heat and mass transfer coefficients is the difficulty of accurately determining the interfacial temperature and concentration of the solution film. Since some uncertainties in determining the interfacial temperature and concentration of the solution film exist, the descriptions of transfer phenomenon near the film surface, especially in the turbulent flow region, are not yet conclusive in the literature. One group of authors [3, 5, 6] assumes that the turbulence (eddy heat transport) is not damped near the film surface. Therefore, there is no temperature gradient existing between the surface and core of the film due to the intensive turbulent heat exchange, and the surface and bulk temperatures are practically equal. Another group of authors [7–10] assumes that turbulence is damped near the surface due to the effect of surface tension or viscosity, so that directly at the interface only molecular transport of heat, mass and momentum is possible. Yüksel and Schlünder [11] directly measured the

NOMENCLATURE

a	thermal diffusivity [$m^2 s^{-1}$]
C	brine concentration by weight [%]
C_p	specific heat capacity [kJ $kg^{-1} K^{-1}$]
D	molecular diffusivity [$m^2 s^{-1}$]
E_T	Ackermann's correction factor, equation (3)
g	gravitational acceleration constant [$m s^{-2}$]
h	enthalpy [kJ kg^{-1}]
k	thermal conductivity [W $m^{-1} K^{-1}$]
L	total film length [m]
Le	Lewis number, Sc/Pr
m_a	local mass absorption rate [kg $s^{-1} m^{-2}$]
M_T	total mass absorption rate per unit width [kg $s^{-1} m^{-1}$]
Nu	Nusselt number
P	pressure [torr]
Pr	Prandtl number v/a
q_a	local heat flux [kW m^{-2}]
Q_T	total heat rate per unit width [kW m^{-1}]
Re	Reynolds number $4\Gamma/\mu$
Sc	Schmidt number v/D
Sh	Sherwood number, equation (14)
T	temperature [K]
x	longitudinal coordinate [m]
U	overall mean heat transfer coefficient [kW $m^{-2} K^{-1}$].

Greek symbols

α	heat transfer coefficient [kW $m^{-2} K^{-1}$]
β	mass transfer coefficient [m s^{-1}]
Γ	flow rate per unit width [kg $s^{-1} m^{-1}$]
δ	film thickness [m]
ΔC_{lm}	logarithmic mean concentration difference, equation (13)
Δh_a	heat of absorption [kJ kg^{-1}]
ΔT_{lm}	logarithmic mean temperature difference, equation (11)
μ	viscosity [kg $s^{-1} m^{-1}$]
v	kinematic viscosity [$m^2 s^{-1}$]
ρ	liquid density [kg m^{-3}].

Subscripts

a	absorption
b	brine
B	bulk condition
c	condensing vapor
fh	film heating
i	inlet
o	outlet
p	plate
ph	film interface
tr	transition
v	water vapor
w	water film.

Superscripts

*	at thermodynamic equilibrium
¯	average.

interfacial temperature of brine film absorbing water vapor by means of the infrared pyrometer. It was shown that the assumption of undamped turbulence near the surface might be improper. They also confirmed the statements of the Levich-type description of falling film heat and mass transfer, that is, the damping of the turbulence occurred not only near the wall but also in the vicinity of the film surface. Furthermore, they proposed a method to calculate

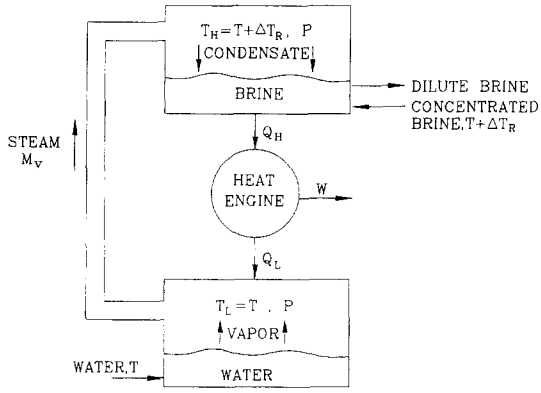

Fig. 1. Schematic description of a concentration difference energy (CDE) power cycle based on external heat transfer surfaces [1].

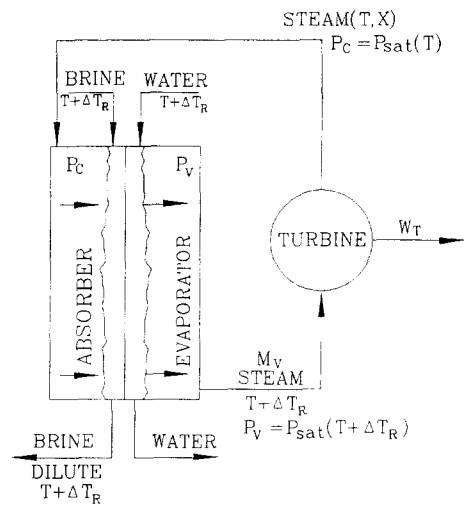

Fig. 2. Schematic description of direct-contact CDE power cycle [3].

the surface temperature and concentration iteratively, which is based on the concept of analogy between heat and mass transfer near the interface. The heat and mass transfer coefficients obtained by this method agreed well with those determined by direct measurement.

In fact, the absorber itself in the above-mentioned CDE power cycle represents an important and well-known film-type heat and mass exchanger. Many theoretical models of heat and mass transfer for the absorber have been developed and many laboratory experiments have been performed [12–17]. However, the results and explanations are inconsistent and partly contradictory, especially the heat transfer coefficient is often anybody's guess.

For investigating the performance characteristics of this new combined absorber–evaporator unit on moderate temperature level, a simulated experimental system is built to test at various operation conditions, namely different solution flow rate, solution concentration, absorber pressure and water flow rate. Moreover, the transfer coefficients on the absorber side are also evaluated, with a goal of understanding the mechanism of heat and mass transfer in a falling film absorber. In that case, the evaporator in the system can be viewed as an effective heat sink to take away the heat generated in the absorber.

2. EXPERIMENTAL APPARATUS AND PROCEDURE

2.1. *Apparatus*

The set-up used in the absorption–evaporation experiments is depicted in Fig. 3. The apparatus mainly consists of: (1) test chamber, (2) a strong solution storage tank, (4) a weak solution storage tank, (5) a tank for water storage, and (3) a condenser for excess vapor and the measuring devices. The test chamber is divided into two compartments by a vertical copper plate 30 cm wide, 100 cm long and 2 mm thick. The left-hand side of the test chamber is used as an absorber and the right-hand side is used as an evaporator. The absorber and the evaporator are linked by an external tube of 50.8 mm in diameter and a pressure regulation valve for vapor transport. In the absorber, coupled heat and mass transfer occurs as the falling film of $CaCl_2$ solution absorbs water vapor. The heat released is transmitted through the copper plate to evaporate the water film in the evaporator side. The vapor generated from the evaporating film is transferred through the pressure regulation valve (RV1), by which the vapor pressure is adjusted to the required pressure level in the absorber compartment. Excess vapor in the absorber is drawn and condensed in the condenser (3).

The strong solution storage tank and the water storage tank are equipped with cooling coils and respective chillers of 2 ton refrigeration capacity. A PID controller is used to control the temperature to within ± 0.1 °C. In addition, the strong solution storage tank is equipped with a 9 kW heating element to regenerate the weak solution after the experiments have been done. The strong brine solution and water are driven by the magnetic-driven pumps to their respective slot-type film distributors. After absorbing the water vapor, the brine solution flows into the weak solution storage tank by gravity. As the brine solution is relatively corrosive, the tanks and the piping system are made of 304 stainless steel.

Thermocouple compression fittings are welded into the desired locations (T1–T13) for use in the measurement of temperatures. The variable-capacitance type pressure transducers are installed in the absorber and evaporator to indicate the absolute vacuum pressure. The accuracy of such sensor is $\pm 0.5\%$ of reading value. Rotameters are used to monitor the liquid flow rates. The specific gravity of the brine solution is measured by means of a digital density meter which is based on the mechanical oscillator technique and a build-in digital thermometer is used in the temperature measurement. The accuracy of the digital density meter is within $\pm 10^{-4}$. From the relationship of specific gravity, temperature and concentration of the $CaCl_2$ solution [18], the brine concentrations can be determined accurately from the measured specific gravity and temperature.

2.2. *Experimental procedure*

The strong brine solution with known concentration and water in the storage tanks are cooled to the required inlet temperatures, respectively. In order to minimize the effect of non-condensible gases, the inert gases should be evacuated from the strong brine solution as much as possible. So, before being pumped to the absorber, the strong brine solution tank is evacuated by a vacuum pump. This purging procedure lasts for about 3 h.

After the purging process, the pressure in the evaporator is gradually brought down by the vacuum pump until the pressure is equal to the saturation pressure corresponding to the inlet water temperature. The liquid films are then uniformly formed over both sides of the vertical plate at the desired flow rates by means of regulating the valves of the by-pass circuits. Evaporation occurs when the pressure in the evaporator reaches the saturation pressure of water film. The generated vapor flows into the absorber through the pressure regulation valve and is absorbed into the falling film of the strong brine solution. The heat of absorption is transmitted through the vertical copper plate to the evaporating water film, continuing to evaporate more water vapor. As the steady-state condition is reached, the following quantities are measured: the flow rates; the pressures; the entrance and exit temperatures of the solution and water; the wall temperatures and the temperatures in the density meter; the density of the concentrated and the diluted solution in the feed and exit, respectively.

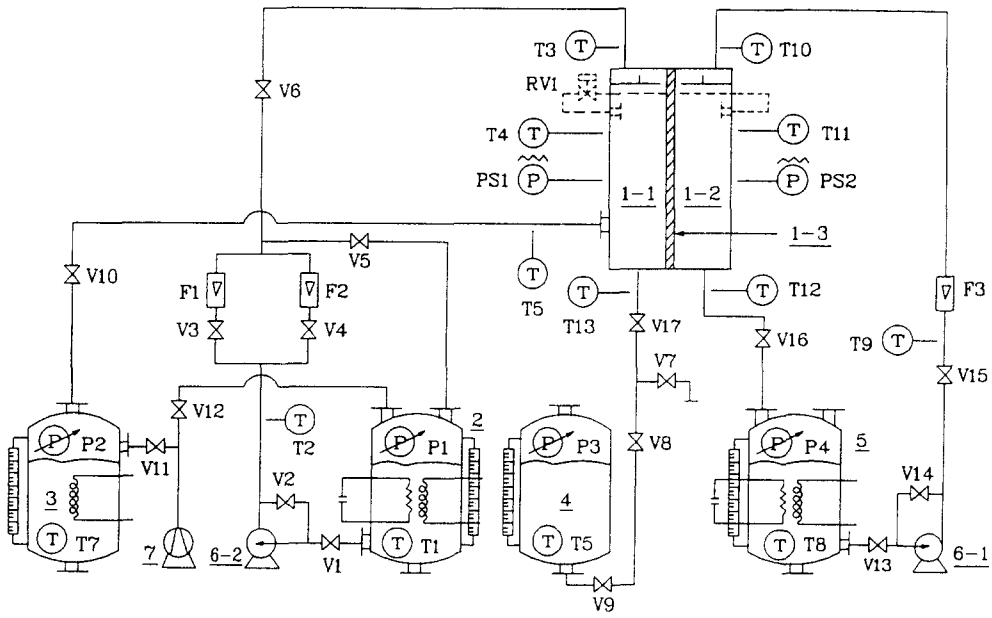

P : pressure gauge (P1–P4)
P : pressure transducer (PS1–PS2)
T : thermocouple (T1–T13)
: pressure regulation valve (RV1)
: rotameter (F1–F3)
: electrical heating element
: control valve (V1–V17)
: cooling coil

Fig. 3. Schematic description of experimental set-up 1-1, absorber; 1-2, evaporator; 1-3, vertical copper plate; 2, storage tank of strong solution; 3, excess vapor condenser; 4, storage tank of weak solution; 5, storage tank of water; 6, liquid pumps; 7, vacuum pump.

3. EVALUATION OF HEAT AND MASS TRANSFER COEFFICIENTS

In absorption of vapor in the brine solution, a large amount of heat of absorption is released at the interface. This results in an increase in the solution temperature, especially in the interfacial temperature, which in turn reduces the vapor solubility. Hence, the absorption rate is controlled significantly by the intensity of heat removal. For the design of the absorber–evaporator unit, heat and mass transfer must be considered simultaneously, since the two are coupled phenomena. Therefore, it is important to determine the interfacial temperature and concentration as evaluating the phenomenon of heat and mass transfer in the present study.

3.1. *Calculation of the interfacial temperature and concentration*

Figure 4 shows a schematic description of the vertical falling film absorber. A brine solution of mass flow rate Γ_{bi}, concentration C_{bi} and temperature T_{bi} enters the absorber and flows down along the vertical plate by gravity. The absorber is filled with water vapor with pressure P_c. The corresponding saturation temperature T_v is lower than the brine temperature

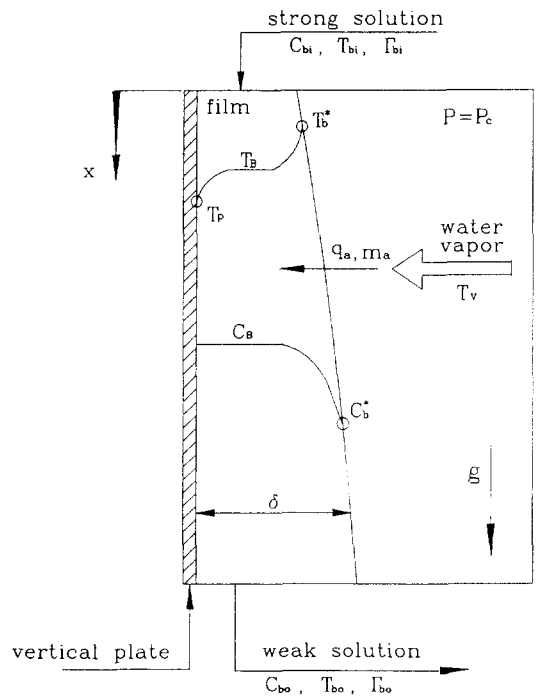

Fig. 4. Film absorption with temperature and concentration profile.

T_b. However, the relatively cold vapor is absorbed and condensed by the brine film, providing P_c is larger than the brine vapor pressure P_b corresponding to T_b and C_b, that is, $P_c > P_b(T_b, C_b)$. As the water vapor is absorbed, the heat of absorption q_a is released at the film surface. Therefore, there are mass flow rates of absorbed water m_a and heat flux q_a transporting from the film surface to the wall simultaneously. Temperature and concentration boundary layers based on the heat and mass transfer near the interface are performed.

Near the interface, the heat transfer coefficient α_{ph} is defined by

$$\alpha_{ph} = \frac{q_a}{(T_b^* - T_B)} \times \frac{1}{E_T} \tag{1}$$

where q_a and the Ackermann's correction factor E_T [19] are given by

$$q_a = m_a(h_v - h_w) = m_a \Delta h_a \tag{2}$$

and

$$E_T = \frac{\Delta h_a \ln[1 + Cp_w(T_b^* - T_B)/\Delta h_a]}{Cp_w(T_b^* - T_B)}. \tag{3}$$

Here, h_v is the enthalpy of water vapor at its temperature T_v, h_w is that of liquid water at the interfacial temperature T_b^*, and Cp_w is the specific heat of liquid water.

The mass transfer coefficient β is defined by regarding the unidirectional mass transport as follows

$$\beta = \frac{m_a}{\rho_b \ln(C_B/C_b^*)} \tag{4}$$

where ρ_b is the density of the brine solution and C_b^* is the interfacial concentration of brine solution at the thermodynamic equilibrium condition, that is

$$C_b^* = C_b^*(T_b^*, P_c). \tag{5}$$

In the experimental work of Yüksel and Schlünder [11], T_b^* was found to be larger than T_B and it was concluded that turbulence is damped in the vicinity of the interface due to the surface tension or viscosity. Therefore, there are only molecular transport of heat, mass and momentum at the interface. Based on these findings, an analogy between heat and mass transfer can be applied to this region:

$$\frac{\alpha_{ph}}{\beta} = \rho_b Cp_b Le^n. \tag{6}$$

The exponent n has a value between 0.5 and 0.6.

From equations (1)–(6), equation (7) can be derived

$$\ln(C_B/C_b^*) = \frac{Cp_b}{Cp_w} Le^n \ln\left[1 + \frac{Cp_w}{\Delta h_a}(T_b^* - T_B)\right]. \tag{7}$$

By using equations (5) and (7), T_b^* and C_b^* can be calculated iteratively by knowing the bulk temperature T_B, bulk concentration C_B and the corresponding physical properties; this would be a proper method for determining T_b^* and C_b^* considering the difficulty of directly measuring them.

3.2. *Definitions of the heat and mass transfer coefficients*

Based on the mass and energy balance, the total heat and mass transfer rate, Q_T and M_T, can be calculated as

$$M_T = \int_0^L m_a \, dx = \Gamma_{bi} \frac{C_{bi} - C_{bo}}{C_{bo}} \tag{8}$$

$$Q_T = M_T h_v + (\Gamma_{bi} h_{bi} - \Gamma_{bo} h_{bo}) \tag{9}$$

respectively, where L is the length of the vertical plate and h_{bi} and h_{bo} are the enthalpies of the inlet and outlet brine solution.

Now, the overall mean heat transfer coefficient U of the absorber–evaporator unit is defined, based on the logarithmic mean temperature difference between the inlet and outlet conditions, as

$$Q_T = UL\Delta T_{lm} \tag{10}$$

where

$$\Delta T_{lm} = \frac{(T_{bi}^* - T_{wi}^*) - (T_{bo}^* - T_{wo}^*)}{\ln\left(\dfrac{T_{bi}^* - T_{wi}^*}{T_{bo}^* - T_{wo}^*}\right)}. \tag{11}$$

The mean mass transfer coefficient $\bar{\beta}$ is defined by the similar method,

$$M_T = \bar{\beta} \rho_b L \Delta C_{lm} \tag{12}$$

$$\Delta C_{lm} = \frac{\ln(C_{bi}/C_{bi}^*) - \ln(C_{bo}/C_{bo}^*)}{\ln\left(\dfrac{\ln(C_{bi}/C_{bi}^*)}{\ln(C_{bo}/C_{bo}^*)}\right)}. \tag{13}$$

In equations (11) and (13), T_{bi}, T_{bo}, C_{bi} and C_{bo} are directly measured from the experiments and T_{wi}^* and T_{wo}^* are the saturation temperatures of the water film corresponding to the pressure in the evaporator; T_{bi}^*, T_{bo}^*, C_{bi}^* and C_{bo}^* are iteratively calculated, as described in Section 3.1, by assuming $T_{Bi} = T_{bi}$, $T_{Bo} = T_{bo}$, $C_{Bi} = C_{bi}$ and $C_{Bo} = C_{bo}$.

4. RESULTS AND DISCUSSION

The present study relates to the following effects: the inlet brine Reynolds number Re_{bi} (100–1300), the inlet brine concentration C_{bi} (35, 40% by weight), the nominal pressure difference for absorption at the brine film interface, $\Delta P = P_c - P_b(T_b, C_b)$ (2.1, 3.1, 4.4, 5.4 torr) and the inlet water Reynolds number Re_{wi} (250–1300). The inlet brine and water temperatures remain constant during the experiments, say $T_{bi} = 20$°C and $T_{wi} = 15$°C, respectively.

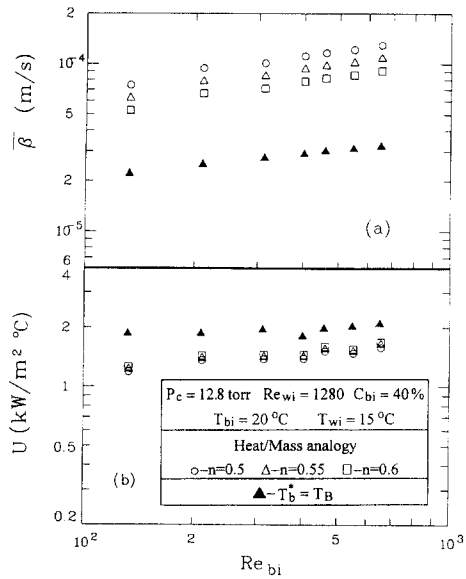

Fig. 5. Comparison of: (a) mean mass transfer coefficient $\bar{\beta}$, (b) overall mean heat transfer coefficient U determined by different methods.

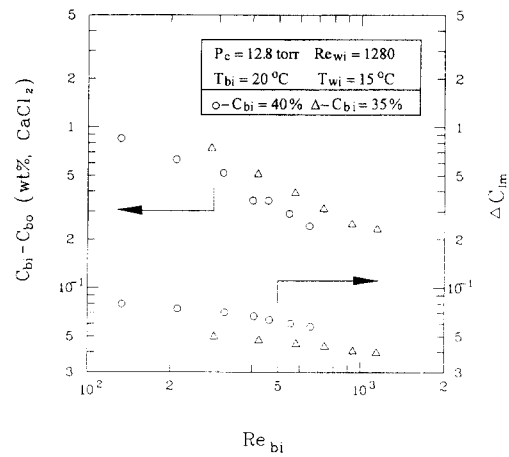

Fig. 6. Effect of inlet brine Reynolds number and inlet brine concentration on the concentration difference and logarithmic mean concentration difference.

4.1. *Comparison of the heat and mass transfer coefficients calculated by different methods*

Figure 5 plots the mean mass transfer coefficient $\bar{\beta}$ and overall mean heat transfer coefficient U as a function of the inlet brine Reynolds number. The absorber pressure P_c is 12.8 torr and the inlet water Reynolds number remains at 1280. As seen in this figure, the assumption that the bulk temperature is equal to the interfacial temperature, $T_b^* = T_B$, would result in an overestimate of ΔC_{lm} and an underestimate of ΔT_{lm}, which in turn leads to unrealistically low $\bar{\beta}$ and high U. The deviations between $\bar{\beta}$, which are determined by means of the method of heat/mass analogy with different exponents n, are about 30%; on the other hand, the exponent n has a relatively small effect on U. The similar results are also concluded in the study of Yüksel and Schlünder [11]. In their experiments, T_b^* measured directly by an infrared pyrometer was found to be generally higher than T_B. They also indicated that $\bar{\beta}$ determined by the infrared pyrometer was always between those which were iteratively calculated with exponent $n = 0.5$ and 0.6, respectively. This means also that the Sh or Nu numbers determined directly by measuring the film surface temperature agree well with those which are evaluated by calculating the surface temperature by use of the heat–mass analogy in the vicinity of the interface. As such, the exponent $n = 0.55$ appears to be a suitable value to calculate the corresponding heat and mass transfer coefficients and is adopted in the present study.

4.2. *Effect of brine flow rate and concentration*

Figure 6 shows the concentration difference between the inlet and outlet brine concentration of the falling film as a function of the inlet brine Reynolds number at two values of the inlet brine concentration. It is noteworthy that the concentration difference, $C_{bi} - C_{bo}$, decreases as the inlet brine Reynolds number increases. The concentration difference also decreases as the inlet brine concentration increases from 35 to 40% (by weight).

The lower part of Fig. 6 presents the effects of the inlet brine Reynolds number and inlet brine concentration on the logarithmic mean concentration difference ΔC_{lm} given by equation (13), which can be regarded as the driving force for the mass transfer in the solution film. The interfacial concentrations C_{bi}^* and C_{bo}^* are calculated by the heat/mass analogy method with $n = 0.55$. Although the outlet brine concentration increases with increasing Re_{bi}, C_{bi}^* and C_{bo}^* increase to a relatively larger extent as Re_{bi} increases. Therefore, ΔC_{lm} only slightly decreases as Re_{bi} increases. This behavior is different from that observed by Brauner *et al.* [3]. In their study, however, T_b^* is assumed to be equal to T_B so that the interfacial brine concentration remains practically constant for a given absorber pressure and inlet brine temperature. On the other hand, an increase in the inlet brine concentration would result in an increase of the driving force for mass transfer.

As depicted in Fig. 7(a), $\bar{\beta}$ would increase when Re_{bi} increases at the two concentration levels. However, the lower inlet brine concentration, $C_{bi} = 35\%$, has a higher mean mass transfer coefficient than that of the larger inlet brine concentration, $C_{bi} = 40\%$. This somewhat unexpected result is reasoned by the following. The higher brine concentration yields a thicker film at a given Re_{bi}, due to the larger value of kinematic viscosity. A thicker brine film obviously causes a higher resistance to heat and mass transfer and thus a lower $\bar{\beta}$. Furthermore, a decrease in diffusion coefficient D_b, corresponding to a higher C_{bi}, also contributed to the decrease of $\bar{\beta}$.

Moreover, the corresponding Sherwood number Sh is defined by

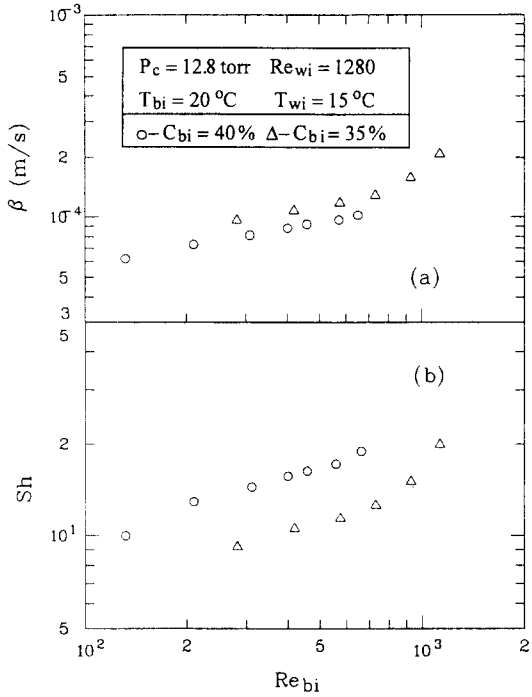

Fig. 7. Effect of inlet brine Reynolds number Re_{bi} and inlet brine concentration on the: (a) mean mass transfer coefficient $\bar{\beta}$, (b) Sherwood number Sh.

$$Sh = \frac{\bar{\beta}(\nu_b^2/g)^{1/3}}{D_b}. \tag{14}$$

Here, the characteristic length $(\nu_b^2/g)^{1/3}$ is chosen to be the length scale of the film thickness. The variation of Sh with the inlet brine concentration level, as shown in Fig. 7(b), is different from that of $\bar{\beta}$. The reason for this difference is due to the fact that ν_b should increase and D_b should decrease with increasing brine concentration, thus enlarging the calculated values of Sherwood numbers.

An examination of the present experimental results shows that the mass transfer coefficient can be correlated by an equation in the following form:

$$Sh/Sc^{0.5} = a \times Re_{bi}^m. \tag{15}$$

The constant a and exponent m can be determined by power regression from the experimental data.

By plotting $Sh/Sc^{0.5}$ vs Re_{bi}, as shown in Fig. 8, the critical Reynolds number for transition from a wavy laminar flow to a turbulent flow seems to be about $(Re_{bi})_{tr} = 700$. This value is lower than 1600, which is obtained in the study of isothermal gas absorption in falling water film by Yih and Chen [20]. The Prandtl number of water is about 5–10 in their study, while the Prandtl number of brine solution is about 20–30 in the present study. Therefore, according to Wilke's conclusion that the transition Reynolds number is proportional to $Pr^{-0.65}$ [21], the decline of $(Re_{bi})_{tr}$ from 1600 to 700 should be reasonable. The correlations of $Sh/Sc^{0.5}$ vs Re_{bi} can be obtained in the two flow regions with $(Re_{bi})_{tr} = 700$.

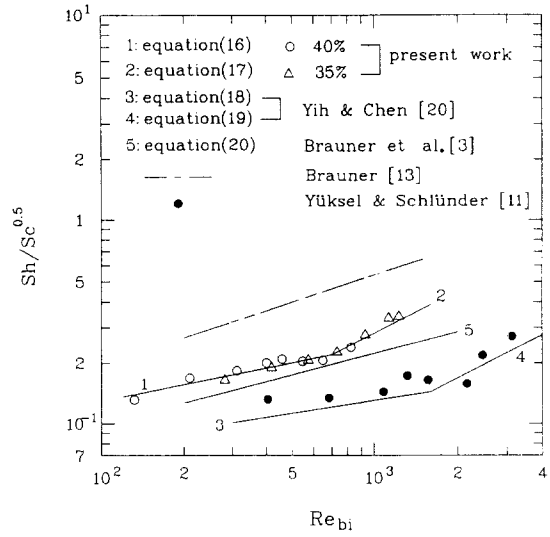

Fig. 8. Comparison of correlations of the mass transfer coefficient.

$$Sh/Sc^{0.5} = 3.725 \times 10^{-2} Re_{bi}^{0.2715}, \quad 100 < Re_{bi} < 700 \tag{16}$$

$$Sh/Sc^{0.5} = 2.326 \times 10^{-3} Re_{bi}^{0.6938}, \quad 700 < Re_{bi} < 1300. \tag{17}$$

In the work of Yih and Chen [20], based on 846 experimental data points on absorption of different gases into water film from the work of 10 investigators in addition to their own, they proposed the following empirical correlation for the mass transfer coefficient:

$$Sh/Sc^{0.5} = 2.995 \times 10^{-2} Re^{0.2134}, \quad 300 < Re \leqslant 1600 \tag{18}$$

$$Sh/Sc^{0.5} = 9.777 \times 10^{-4} Re^{0.6804}, \quad 1600 < Re < 10\,500. \tag{19}$$

Comparing equation (16) with (18) and equation (17) with (19), it is found that the constant a and exponent m of the present correlations are slightly higher. It seems to be attributed to the lateral convective term in the diffusion equation. The effect of the mean molar velocity across the direction of the film flow on the absorption of sparingly soluble gases (isothermal absorption) is less significant. However, on the absorption of high soluble water vapor into brine film (non-isothermal absorption), like the present study, the mass transfer rate is not low enough to neglect such an effect. In Brauner's theoretical analysis [13], the problem of non-isothermal vapor absorption into brine film was considered. He concluded that the transfer rate would be significantly augmented due to the convective effect arising from finite absorbate dilution. Brauner *et al.* [3] also conducted the experiments to measure the mass transfer coefficient of non-isothermal vapor absorption on a vertical plate. The correlation obtained in their work was

$$Sh/Sc^{0.5} = 0.02Re_{bi}^{0.35}. \quad (20)$$

The correlations mentioned above together with the numerically obtained results from Brauner [13] are presented in Fig. 8. Care should be given to equation (20), wherein T_b^* is assumed to be equal to T_B, which would yield a lower mass transfer coefficient, as discussed in Section 4.1. As can be seen in Fig. 8, the mass transfer coefficients predicted numerically by Brauner [13] are higher than those in the present study, while those obtained by Yüksel and Schlünder [11] are lower.

Moreover, a tube of 2.72 cm OD and 212 cm long was used as the wetted wall in the experiment of Yih and Chen [20], but the wetted wall is a flat plate 30 cm wide and 100 cm long in the present experiment. Since the waviness of the film is damped by the curvature of the tube wall, the mass transfer coefficient is decreased [22]. The reduced length of the wetted wall could increase the mass transfer coefficient when the thermal entrance effect is taken into account. In the work of Yüksel and Schlünder [11], a tube 250 cm long was utilized as the wetted wall and the Prandtl number is 7.4. These conditions are similar to those of Yih and Chen. However, the values of $Sh/Sc^{0.5}$ gained in the experiments of Yüksel and Schlünder are still about 20% higher than those of Yih and Chen.

Another important quantity of interest is the total mass transfer rate M_T of water vapor absorbed into the brine film. As shown in Fig. 9, increasing the inlet brine flow rate would only effect a slight increase in M_T except at the higher Re_{bi}. Generally speaking, the variation of M_T is small within the current range of Re_{bi}. The reason for this behavior is that although a higher Re_{bi} will raise the mean mass transfer coefficient, it also yields a smaller driving force ΔC_{lm}. In addition, the effect of increasing the inlet brine concentration is to reduce M_T, which is consistent with the corresponding decrease in the concentration difference, $C_{bi}-C_{bo}$, for a higher inlet brine concentration, as shown in Fig. 6.

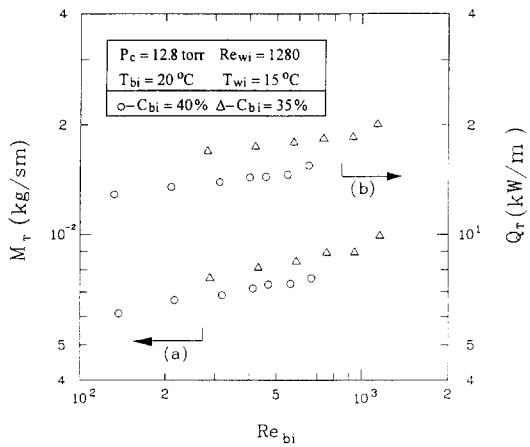

Fig. 9. Effect of inlet brine Reynolds number Re_{bi} and inlet brine concentration on the: (a) total absorption rate M_T, (b) total heat transfer rate Q_T.

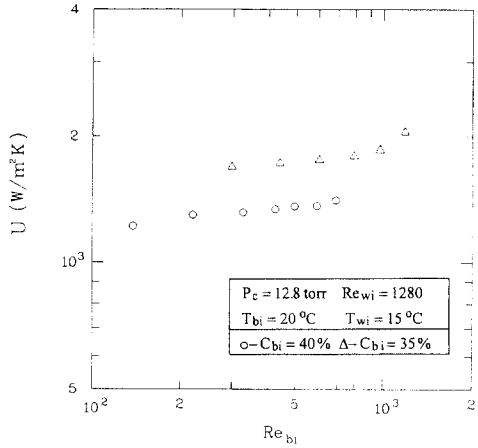

Fig. 10. Effect of inlet brine Reynolds number Re_{bi} and inlet brine concentration on the total mean heat transfer coefficient U.

With regard to the characteristics of heat transfer, the effect of the inlet brine concentration is like that on the mass transfer. That is, a higher C_{bi} leads to a larger logarithmic mean temperature difference ΔT_{lm} (represents the driving force for heat transfer) but less overall heat transfer coefficient U, as shown in Fig. 10, and total heat transfer rate Q_T. Moreover, the inlet brine Reynolds number has a minimum effect on ΔT_{lm}. The overall heat transfer coefficient remains fairly constant with respect to Re_{bi}, except for the higher Re_{bi} where U would increase with increasing Re_{bi}. Actually, the overall heat transfer coefficient U represents the resistance of heat transfer from the absorber side to the evaporator side. Therefore, it is difficult to find a suitable characteristic length and thermal conductivity to obtain a corresponding non-dimensional heat transfer coefficient.

4.3. *Effect of vapor pressure of absorber*

As mentioned earlier, the relatively cold vapor is absorbed and condensed by the hot brine film, provided the vapor pressure P_c is larger than the vapor pressure of the brine solution $P_b(T_b, C_b)$. Therefore, the pressure difference, $\Delta P = P_c - P_b$, would be an important parameter in the present study. The inlet brine concentration and temperature remain at $C_{bi} = 35\%$ and $T_{bi} = 20°C$ and the corresponding saturation pressure of the brine solution is $P_b(35\%, 20°C) = 8.4$ torr. The generating vapor in the evaporator is transported through the vapor regulation valve, by which the pressure of vapor entering the absorber is adjusted to three desired levels: 12.8, 11.5 and 10.5 torr, respectively.

As shown in Fig. 11(a), increasing the absorber pressure, that is, a larger pressure difference ΔP, would result in an increase of ΔC_{lm}. In other words, the condensation driving force and the solution potential for absorbing vapor increase as ΔP increases. Based on the measured and iteratively calculated data, $Sh/Sc^{0.5}$ is plotted in Fig. 11(b). It can be seen that the

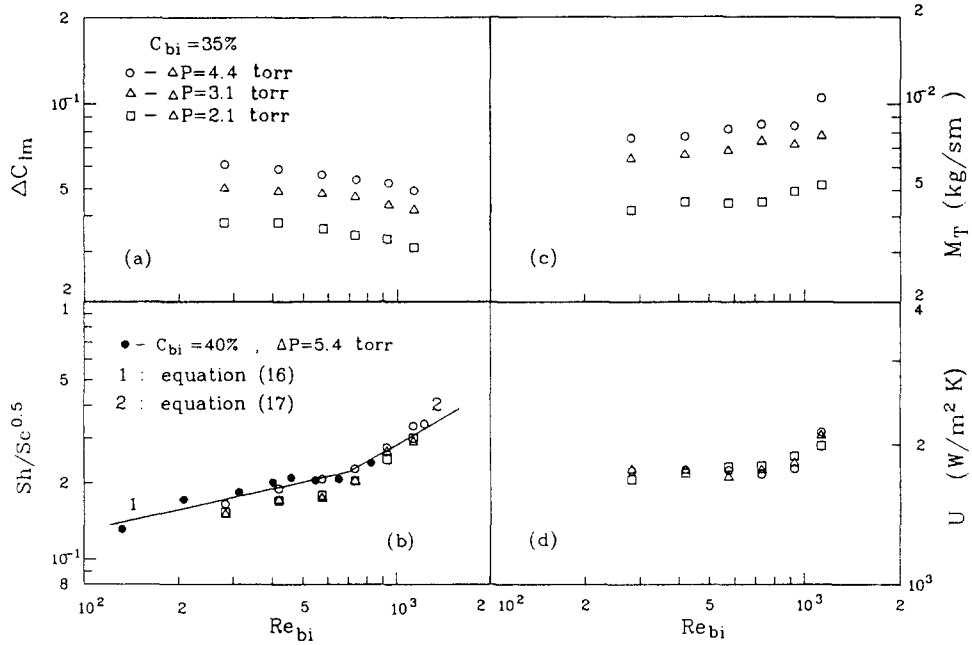

Fig. 11. Effect of absorber pressure on : (a)logarithmic mean concentration difference, (b) $Sh/Sc^{0.5}$, (c) total mass transfer rate, (d) overall mean heat transfer coefficient.

variation of ΔP has a negligible effect on the mean mass transfer coefficient and the values of $Sh/Sc^{0.5}$ for different ΔP agree well with equations (16) and (17) obtained in Section 4.2. This implies that the absorption (condensation) process in the present study is mainly controlled by a mass transfer mechanism on the liquid side. Accordingly, the mean mass transfer coefficient depends on the physical properties and the flow pattern, but it would be independent of the absorber pressure. As expected, the total mass transfer rate decreases with decreasing P_c in the condition that ΔC_{lm} decreases as P_c decreases, but $\bar{\beta}$ does not change with P_c.

The influence of absorber pressure on the behavior of heat transfer is similar to that of mass transfer. The logarithmic mean temperature difference and the total heat transfer rate altogether decrease as P_c decreases. The overall mean heat transfer coefficient U remains practically constant as P_c changes, as shown in Fig. 11(d).

4.4. *Heat transfer coefficient on absorber*

In addition to the overall mean heat transfer coefficient U, the heat transfer coefficient on the absorber side is also an important value to be known, which represents the resistance of heat transfer from the brine film interface to the vertical plate. The mean heat transfer coefficient on the absorption side $\bar{\alpha}_a$ can be defined as, similarly to U,

$$\bar{\alpha}_a = \frac{Q_T}{L\Delta T_{lm,a}} \tag{21}$$

and

$$\Delta T_{lm,a} = \frac{(T^*_{bi} - T_{pi}) - (T^*_{bo} - T_{po})}{\ln\left(\dfrac{T^*_{bi} - T_{pi}}{T^*_{bo} - T_{po}}\right)} \tag{22}$$

where T_{pi} and T_{po} are the temperatures on top and bottom of the plate, which are measured by thermocouples.

From the experimental data, it is found that $\Delta T_{lm,a}$ and $\bar{\alpha}_a$ are, respectively, approximately equal to ΔT_{lm} and U obtained for the whole unit. To further resolve this result, the flow rate of water in the evaporator is changed to investigate the effect of inlet water Reynolds number Re_{wi}. As shown in Fig. 12, Re_{wi} has negligible influence on both $\bar{\beta}$ and U. Therefore, the

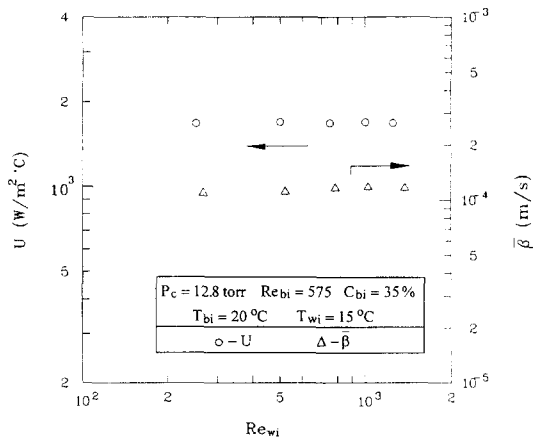

Fig. 12. Effect of inlet water Reynolds number Re_{wi} on mean mass transfer coefficient $\bar{\beta}$ and overall mean heat transfer coefficient U.

water flow rate only has a minor effect on the performance of such a combined absorber–evaporator exchanger.

Accordingly, a non-dimensional heat transfer coefficient (Nusselt number) for the vapor absorption can be defined as

$$Nu = \frac{\overline{\alpha_a}(\nu_b^2/g)^{1/3}}{k_b} \tag{23}$$

where k_b is the thermal conductivity of brine solution.

With regard to the relationship between Nu, Re_{bi} and Pr, a commonly used form $Nu = \text{const.} \times Re_{bi}^m Pr^n$ is first tested. However, an attempt to find the suitable values of exponents m and n to correlate all of the experimental data does not succeed. A similar conclusion is also made in the study of Yüksel and Schlünder [23]. Therefore, it can be implied that the characteristics of heat transfer near the film surface and near the wall are different. Based on this argument, a new model to evaluate the Nusselt number is proposed in this work,

$$\frac{1}{Nu} = \frac{1}{Nu_{ph}} + \frac{1}{Nu_p} \times \frac{1}{S} \tag{24}$$

where Nu_{ph} is the Nusselt number near the film surface, Nu_p the Nusselt number near the wetted wall and S a correction factor.

Remembering that there exists an analogy between heat and mass transfer near the film surface, Nu_{ph} can be calculated as

$$Nu_{ph} = ShLe^{n-1} \tag{25}$$

where Le is the Lewis number and $n = 0.55$ in this work. Furthermore, from equations (16), (17) and (25) the following correlations can be derived:

$$Nu_{ph} = 3.725 \times 10^{-2} Re_{bi}^{0.2715} Pr^{0.45} Sc^{0.05}, \quad 100 < Re_{bi} < 700 \tag{26}$$

$$Nu_{ph} = 2.326 \times 10^{-3} Re_{bi}^{0.6938} Pr^{0.45} Sc^{0.05}, \quad 700 < Re_{bi} < 1300. \tag{27}$$

Near the region of the wetted wall, only heat transfer with no phase change occurs and mass transfer does not exist. Regarding the experimental studies on such a problem of film heating or cooling, Wilke's work [21] is noted, in which the experimental results encompassing a wide range of Prandtl numbers (5.4–210) and Reynolds numbers were reported. Wilke measured the heat transfer coefficient of a liquid film flowing downwards on the outside of a 240 cm length and 4.2 cm diameter vertical tube heated internally by hot water. The empirical equations obtained by Wilke can be transformed into relations between Nusselt number (Nu_{fh} for film heating) and film Reynolds number by introducing the film thickness δ derived by Nusselt for $Re < 1600$ and that given by Brauer [24] for $Re \geqslant 1600$, that is,

$$\delta = 0.91(\nu^2/g)^{1/3} Re^{1/3}, \quad Re < 1600 \tag{28}$$

$$\delta = 0.2077(\nu^2/g)^{1/3} Re^{8/15}, \quad Re \geqslant 1600. \tag{29}$$

The resultant correlations are expressed as

$$Nu_{fh} = 2.066 Re^{-1/3}, \quad Re < 2460 Pr^{-0.646} \tag{30}$$

$$Nu_{fh} = 0.0323 Re^{1/5} Pr^{0.344}, \quad 2460 Pr^{-0.646} \leqslant Re < 1600 \tag{31}$$

$$Nu_{fh} = 0.0011 Re^{2/3} Pr^{0.344}, \quad 1600 \leqslant Re < 3200 \tag{32}$$

$$Nu_{fh} = 0.0087 Re^{2/5} Pr^{0.344}, \quad Re \geqslant 3200. \tag{33}$$

Equations (30)–(33) can be applied to calculate the Nusselt number near the wall Nu_p in equation (24).

The correction factor S in equation (24) is an experimentally determined value. It is affected by the following factors: (1) the design of the feeding device (film distributor) and its strong effect on the heat transfer in the entrance region; (2) geometrical conditions including the type (tube or plate) and length of the wetted wall and the diameter of the tube; (3) the effect of three molecular diffusivities on the relative thickness of hydrodynamic, thermal and concentration boundary layers. In this work, a suitable value for the correction factor S is found to be 1.3 to correlate all of the experimental data.

Figure 13 shows the ratio of the Nusselt number obtained by equation (24) to that determined by experimental measurement. The experimental data of Yüksel and Schlünder [11] is also recalculated and depicted in this figure by substituting their own Sh into equation (25) and a different correction factor $S = 0.9$. The value of this Nusselt number ratio falls into the range of 0.85–1.15 and the average deviation is about 8%. The reasonably good agreement indicates the potential usage of equation (24) to evaluate

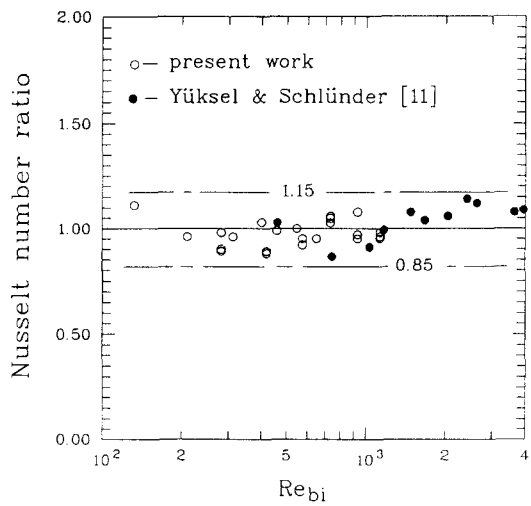

Fig. 13. Comparison of the Nusselt number ratio predicted by equation (24) to that determined by experiments.

the heat transfer coefficient in the problem of non-isothermal film absorption. We remark, however, that the application of the model proposed in the present study needs further validation with more experimental results, especially a further insight into the correction factor S.

5. CONCLUSION

The heat and mass transfer characteristics of a new combined vertical film-type absorber–evaporator heat exchanger is experimentally investigated. The experimental parameters involved in this process, including the flow rates of the inlet brine solution and pure water, the inlet brine concentration and the pressure difference in the absorber, are examined. The method of analogy between heat and mass transfer near the film surface is used to iteratively calculate the interfacial temperature and concentration of the brine film and the mass and heat transfer coefficients are accordingly determined. The important results are summarized as follows:

(1) Based on the experimental data, the correlation of mass transfer coefficient has been derived, namely equations (16) and (17), with the transitional Reynolds number of about 700. The values of $Sh/Sc^{0.5}$ are larger than those obtained in the isothermal absorption of sparingly soluble gas, although they have a similar trend with respect to the film Reynolds number.

(2) The overall mean heat transfer coefficient remains practically constant compared to the inlet brine Reynolds number Re_{bi} and the absorber pressure level, except for the higher Re_{bi} where U increases with increasing Re_{bi}.

(3) Considering the different characteristics of heat transfer between the film surface region and wall region, a new model has been proposed and successfully applied to evaluate the heat transfer coefficient of the absorber itself.

Acknowledgements—The authors acknowledge the discussion with Professor Chen-Yen Cheng. The authors are also grateful to Professor Neima Brauner for his kind offer of the physical properties of $CaCl_2$ solution. The financial support by the National Science Council, Republic of China under contract NSC 84-2212-E-002-011 is also gratefully acknowledged.

REFERENCES

1. Isshiki, N., Study on the concentration difference energy system. *Journal of Nonequilibrium Thermodynamics*, 1977, **2**, 88–107.
2. Brauner, N., Moalem Maron, D. and Sideman, S., Simultaneously mass and heat transfer in direct contact hygroscopic condensation. *Proceedings of the Eighth International Heat Transfer Conference*, Vol. 4, pp. 1647–1652, San Francisco, 1986.
3. Brauner, N., Moalem Maron, D. and Harel, Z., Experimental studies of a hygroscopic condenser–evaporator heat exchanger based on condensation differences of vertically falling films. *Experimental Thermal and Fluid Science*, 1989, **2**, 392–409.
4. Cheng, C. Y., Multiple Effect Absorption Refrigeration Processes and Apparatuses for Use Therein, US Patent No. 5061306, 1991.
5. Limberg, H., Wärmeübergan an Turblente und Laminare Rieselfilme. *International Journal of Heat and Mass Transfer*, 1973, **16**, 1691–1702.
6. Yih, S. M. and Liu, J. L., Prediction of heat transfer in turbulent falling liquid films with or without interfacial shear. *AIChE Journal*, 1983, **29**, 903–909.
7. Lamourelle, A. P. and Sandall, O. C., Gas absorption into a turbulent liquid films. *Chemical Engineering Science*, 1972, **27**, 1035–1043.
8. Mills, A. F. and Chung, D. K., Heat transfer across turbulent falling film. *International Journal of Heat and Mass Transfer*, 1973, **16**, 694–696.
9. Grossman, G. and Heath, M., Simultaneous heat and mass transfer in absorption of gases in turbulent liquid films. *International Journal of Heat and Mass Transfer*, 1984, **27**, 2365–2376.
10. Mudawwar, I. A. and El-Marsi, M. A., Momentum and heat transfer across freely-falling turbulent liquid films. *International Journal of Multiphase Flow*, 1986, **12**, 771–790.
11. Yüksel, M. L. and Schlünder, E. U., Heat and mass transfer in non-isothermal absorption of gases in falling liquid films, part I: experimental determination of heat and mass transfer coefficients. *Chemical Engineering Process*, 1987, **22**, 193–202.
12. Grossman, G., Heat and mass transfer in film absorption. In *Handbook of Heat and Mass Transfer*, ed. P. C. Nicholas. Gulf, Houston, TX, 1986, Chap. 6.
13. Brauner, N., Non-isothermal vapour absorption into falling film. *International Journal of Heat and Mass Transfer*, 1991, **34**, 767–784.
14. Grigor'eva, N. I. and Nakoryakov, V. E., Combined heat and mass transfer during absorption in drops and films. *Journal of Engineering Physics*, 1977, **32**, 243–247.
15. Nakoa, K., Ozaki, E. and Yamanaka, G., Study on vertical type absorber for absorption heat transfer. In *Heat and Mass Transfer in Refrigeration and Cryogenics*, eds. J. Bougard and N. Afgan. Hemisphere, Washington, DC, 1987, pp. 214–231.
16. Matsuda, A., Choi, K. H., Hada, K. and Kawamura, T., Effect of pressure and concentration on performance of a vertical falling-film type of absorber and generator using lithium bromide aqueous solution. *International Journal of Refrigeration*, 1994, **17**, 538–542.
17. William, A. M. and Horacio, P. B., Vertical-tube aqueous LiBr falling film absorption using advanced surfaces. *International Absorption Heat Pump Conference*. New Orleans, 1994, pp. 185–202.
18. Feist, E. M., Physical properties of salt solutions (Compilation of data). Negev Research Institute, Solar Pond Project, 1950.
19. Bird, R. B., Stewart, W. E. and Lightfoot, E. N., *Transport Phenomena*. Wiley, New York, 1965.
20. Yih, S. M. and Chen, K. Y., Gas absorption into wavy and turbulent falling liquid films in a wetted-wall column. *Chemical Engineering Communication*, 1982, **17**, 123–136.
21. Wilke, W., Wärmeübergang an Rieselfilme. *Forschung Hefte Verein Deutsch Ingenieur*, 1962, **490**, B28.
22. Yih, S. M., Modeling heat and mass transport in falling liquid film. In *Handbook of Heat and Mass Transfer*, ed. P. C. Nicholas. Gulf, Houston, TX, 1986, Chap. 5.
23. Yüksel, M. L. and Schlünder, E. U., Heat and mass transfer in non-isothermal absorption of gases in falling liquid films, part II: theoretical description and numerical calculation of turbulent falling film heat and mass transfer. *Chemical Engineering Processing*, 1987, **22**, 203–213.
24. Brauer, H., Strömung und Wärmeübergang bei Rieselfillmen. *Forschung Hefte Verein Deutsch Ingenieur*, 1956, **457**, B22.